Discovery of TRAF-2 and NCK-interacting kinase (TNIK) inhibitors by ligand-based virtual screening methods

Anna Bujak[a,b,#], Filip Stefaniak[a,#,∞], Daria Zdzalik[a, #,*,∞], Paulina Grygielewicz[a,b], Barbara Dymek[a], Marcin Zagozda[a], Pawel Gunerka[a,c], Monika Lamparska-Przybysz[a], Krzysztof Dubiel[a], Maciej Wieczorek[a], Karolina Dzwonek[a,d]

[a]Innovative Drugs R&D Department, Celon Pharma Inc., Mokra 41a, 05-092 Lomianki/Kielpin, Poland; [b]Postgraduate School of Molecular Medicine, Zwirki i Wigury 61, 02-091 Warsaw, Poland; [c]Medical University of Lodz, Kosciuszki 4, 90-419 Lodz, Poland; [d]Department of Immunology, Center for Biostructure Research, Medical University of Warsaw, Banacha 1a, F Building, 02-097 Warsaw, Poland

[#] These authors contributed equally to this work

*To whom correspondence should be addressed:

Daria Zdzalik, Innovative Drugs R&D Department, Celon Pharma Inc., Mokra 41a, 05-092 Lomianki/Kielpin, Poland

Tel.: +48603804317 Fax: +48 227517477

Email: dariazdzalik@wp.pl

Present Address:

[∞] International Institute of Molecular and Cell Biology in Warsaw, 4 Ks.

Trojdena Street, 02-109 Warsaw, Poland

Abstract

TRAF-2 and NCK-interacting kinase (TNIK) is a serine-threonine kinase with a proposed role in Wnt/β-catenin and JNK pathways. Due to its implication in Wnt-mediated colorectal carcinogenesis, selective TNIK inhibition has emerged as an attractive anti-cancer therapeutic strategy. So far, only few TNIK inhibitors have been described and none of them reached advanced preclinical development.

In this study, a virtual screening approach was applied for investigation of novel TNIK inhibitors. The best performing ShaEP methodology for similarity searching was applied for screening of a commercially available small molecules database. Among several discovered TNIK kinase inhibitors, a compound containing the furan-2-carboxamide scaffold was found to be the most active, with $IC_{50} = 0.85$ μM. An advanced substructure search led to the discovery of a more potent and selective compound with $IC_{50} = 258$ nM. The most active compounds were tested *in vitro* for their effect on Wnt/β-catenin pathway and proliferation of Wnt-active colorectal cancer cells.

The compounds identified in this study represent attractive starting points for the development of more potent and selective small molecule TNIK inhibitors for both therapeutic application and research on TNIK biological role.

2

Introduction

Traf-2 and NCK-interacting kinase (TNIK) was described for the first time in 1999 by Fu et al. as a novel serine/threonine kinase belonging to the family of germinal center kinases (GCK)[1]. TNIK was shown to specifically activate the c-Jun N-terminal kinase (JNK) pathway and its role in the regulation of cytoskeleton was suggested[1]. Several following studies focused on the contribution of TNIK in Wnt/β-catenin signaling and its function in tumorigenesis. It was found that TNIK directly binds to TCF4 and β-catenin and, through phosphorylation of TCF4, promotes Wnt target genes activation[2]. Since aberrant activation of TCF4/β-catenin transcriptional program leads to various types of cancer, especially located in the intestine, inhibition of Wnt/β-catenin pathway became an attractive therapeutic strategy for the treatment of colorectal cancer[2]. TNIK was proven to be essential for growth of colon cancer cell lines and its knockdown in these cell lines caused considerable inhibition of cell proliferation[3]. The TCF/LEF transcription activity decreased following *TNIK* gene expression silencing[2, 4], and TNIK overexpression was shown to activate the canonical Wnt signaling pathway[5]. TNIK was also reported to play a significant role in proliferation and differentiation of leukemia stem cells, in which BCR-ABL and CD27 signaling co-activates β-catenin/TNIK induced expression of Wnt target genes driving chronic myeloid leukemia progression[6]. Additionally, TNIK was proven to be mandatory for proliferation and survival of EBV-transformed B-cells due to activation of NF-κB and JNK signaling by interaction with the major EBV oncoprotein LMP1 and its cellular counterpart, the B-cell co-stimulatory receptor CD40[7]. What is important from the drug discovery point of view, TNIK was suggested as a novel therapeutic target in TNIK-amplified gastric cancer[8] and epithelial-mesenchymal transition associated disorders such as cancer metastasis and fibrosis[9]. These findings brought much interest in the development of small-molecule TNIK inhibitors. First report on TNIK inhibitors and their use was provided by Yamada et al. (2010)[4], and followed by the discovery of 4-phenyl-2-phenylaminopyridine-based inhibitors reported by Ho et al. (2013)[10]. In the most recent study, Kim et al. (2014) described a novel aminothiazole KY-05009 with potential to

3

inhibit TNIK [9]. So far, none of these compounds entered clinical trials or became commercially available for research use, therefore, there is still a need for new discoveries in this field.

In this study, we used virtual screening to discover small-molecule inhibitors of TNIK kinase. This strategy has been widely applied in the discovery of lead compounds in the initial stage of drug development. Two main classes of methods can be distinguished: a receptor-based methods, which utilize the known structure of the target macromolecule[16-18] and ligand-based methods, where the structure of known active compounds is used as a template for searching or designing new ligands[19-21]. The hit identification performance of the screening methods varies depending on the target, thus choosing an appropriate algorithm is necessary prior to virtual screening campaign[12, 13, 22, 23]. To our best knowledge, there are no reported data on applying these computational tools for discovery of TNIK inhibitors. Thus, the initial benchmarking of available methods was necessary. We have successfully identified five novel hit compounds that in concentration of 10 μM inhibited more than 50% of TNIK kinase activity. Two of the most potent compounds with furan-2-carboxamide scaffold were further subjected to *in vitro* cell-based assays to test their effect on Wnt/β-catenin signaling and viability of Wnt-active colorectal cancer cells.

Results and discussion

Evaluation of virtual screening methods

To select the optimal screening method, an initial benchmark of available tools was performed. For this purpose, the testing dataset composed of 30 compounds active against TNIK extracted from ChemBlDb database and 1486 inactive compounds (either true negatives extracted from ChemBlDb or putative negatives generated according to DUD-E methodology) was constructed. For a list of ChemBl identifiers, PubMed identifiers and literature references of true positive and true negative compounds used in a testing dataset are listed in the Supplementary Table S1. There are several approaches to quantify virtual screening performance. Here, two well-known metrics

were used in parallel. The first was Enrichment Factor (EF) that evaluates the ability of a tool to put active compounds at the top n% of the ranked list[24], EF for n=10% was used ($EF_{10\%}$). Second metric used in this study was BEDROC (Boltzmann-Enhanced Discrimination of ROC) which combines actives enrichment factor with ability of early hit recognition[25]. Weighting parameter α for BEDROC was 20.

Structure-based methods

The structure based screening methods included molecular docking with AutoDock Vina[26]. Up to date, there is only one crystal structure of TNIK kinase deposited in the Protein Data Bank (PDB: 2X7F). To evaluate this screening method, testing compounds were docked independently to three different structures of TNIK kinase domain (chains: A, B and C). However, the performance expressed in low $EF_{10\%}$ and BEDROC was poor.

Ligand-based methods

In the ligand-based methods, three known kinase inhibitors were used independently as search patterns: doramapimod, dovitinib and sunitinib. The template inhibitors were selected based on their high affinity to kinase domain of TNIK, since all of them displayed nanomolar dissociation constant (K_d) values (Fig. 1)[27]. 2D fingerprint similarity methods included 12 different fingerprint types, but there was no clear leader. The best $EF_{10\%}$ = 5 was reached for CDK Standard Fingerprint (1024 bit path based, hashed fingerprint) and MACCS (166 bit structural keys), however BEDROC was 0.20 and 0.16 respectively. The best BEDROC value of 0.31 was reached for PubChem fingerprint (881 bit structural keys) with moderate $EF_{10\%}$ = 4.

In the ligand-based methods group, which utilize 3D structure of compounds, three programs were tested. Align-it superimposes rigid molecules according to their pharmacophores[28]. SHAFTS utilizes a hybrid similarity metric combined with molecular shape and labelled chemistry groups annotated by pharmacophore features[29]. In both cases the performance was not satisfactory. The best results - for ligand-based methods and for all methods tested - were obtained with ShaEP

5

program. It aligns two rigid structures and computes a similarity of the overlay. The superimposition is achieved by finding similarities in the molecular electrostatic potential field (MEP), which results in a group of candidate overlays. Next, the volume overlap of the structures and the MEPs are maximized[30]. As the partial charges are essential for this algorithm, four charge models were tested: EEM (electronegativity equalization method atomic partial charges), QEq (charge equilibration partial charges), QTPIE (charge transfer, polarization and equilibration partial charges) and Gasteiger-Marsili. A detailed benchmark results for each template/charge model setup is shown in the Supplementary Table S2. The best results were achieved for EEM charges model and dovitinib as a template, with BEDROC = 0.33 and $EF_{10\%}$ = 5. This setup was used for virtual screening of the compounds library.

Virtual screening

The Zelinsky Institute database (HTS stock) was filtered using simple physiochemical descriptors: molecular weight and TPSA. Resulting subset was screened using ShaEP with dovitinib as a template. In the next step, 500 top-scored compounds were compared to internal database of known kinase inhibitors to exclude compounds with already known scaffolds. Resulting subset was inspected visually and 296 diverse compounds were selected for further activity evaluation (Supplementary Table S3).

Hit identification and evaluation

In vitro kinase inhibition assay

To directly verify the inhibitory potency of virtual hits, selected top-scored compounds were purchased from The Zelinsky Institute.The inhibitory activity of selected compounds against TNIK kinase was evaluated in biochemical assay at concentration of 10 μM using recombinant enzyme (Supplementary Table S3). Five compounds displayed TNIK inhibition above 50% and were selected for the determination of IC_{50} values. Activity of tested compounds and IC_{50} values of the most active ones are shown in Fig. 3 and Table 1, respectively. All newly identified hit

6

compounds represent diversified chemical structures that were not previously reported as TNIK inhibitors. Moreover, the identified compounds display low molecular weight, which is a good starting point for further chemical optimization.

One of the tested compounds showed the IC_{50} value higher than 10 μM, three compounds had the IC_{50} in the range of 1 μM to 10 μM, and one compound showed a submicromolar IC_{50} value against TNIK (Table 1). The most potent compound 3 (5-(2,5-dichlorophenyl)-*N*-[4-(4-methylpiperazin-1-yl)phenyl]furan-2-carboxamide) displayed IC_{50} = 0.85 μM. This compound has a scaffold identical to previously described MK2 inhibitors. It was suggested that these compounds are the non-ATP-competitive inhibitors of MK2 kinase as they did not show relevant IC_{50} shift when tested in the kinase inhibition *in vitro* assay at low versus high ATP concentrations[31]. In order to verify whether our hit compound 3 is an ATP-competitive or a non-ATP-competitive inhibitor of TNIK, we performed kinase inhibition assay in the presence of increasing ATP concentrations. The observed increase in IC_{50} value was similar to that of an ATP-competitive inhibitor dovitinib (Fig. 4A, 4B). This implies that compound 3 is likely an ATP-competitive TNIK inhibitor that inhibits the kinase activity via occupation of the ATP-binding pocket of the kinase domain.

For chemical space exploration, The Zelinsky Institute database was searched for structural analogs of the compound 3 using substructure search and fingerprint similarities. The series of new compounds were identified and tested. Among 14 compounds containing furan-2-carboxamide scaffold only compound 3a (5-(3-chloro-2-methylphenyl)-*N*-(4-sulfamoylphenyl)furan-2-carboxamide) displayed significant activity with IC_{50} = 258 nM (Table 2, Fig. 4C).

For *in vitro* drug selectivity evaluation, the hit compounds 3 and 3a were examined against a panel of human kinases. No significant inhibition was detected against ALK, AURA, BTK, EGFR, FGFR1, GSK3β, IGF-1R, JAK2, PI3Kα, and SYK kinases (Table 3). It is of note that the compounds displayed little activity against FGFR1 even though dovitinib, used as a template for

7

virtual screening, is a multitarget kinase inhibitor with high potency against FGFR1-3 kinase [32]. Additionally, compound 3a had improved selectivity against FLT3, PDGFRβ and KDR compared with both dovitinib and compound 3[27].

Docking analysis

In order to define the binding mode of our hit, we docked compound 3 into the ATP-binding site of TNIK kinase. Following the visual analysis of the obtained docking poses, we chose the most convincing (however, not the highest scored) binding mode. Predicted binding interaction between compound 3 and TNIK is shown in Fig. 5. According to this docking model, furan-2-carboxamide group is situated in the adenine binding region. The 2,5-dichlorophenyl group occupies hydrophobic back pockets located near the gk (gatekeeper) residue (Met105), while the 4-methylpiperazine group extends toward the solvent-exposed region. The hydrogen atom of amide NH group forms key hydrogen bond with backbone carbonyl group of Cys108 (2.5 Å), a gk+3 residue located in the hinge region of the ATP-binding pocket. An additional weak H-bond with hinge residue gk+1 probably occurs between hydrogen atom in C4 position of the furan ring and backbone carbonyl group of Glu106 with a distance of 3.6 Å. No hydrogen bond is possible between atom in C3 position of the furan ring and hydrogen atom of backbone NH group of Cys108. However, C3 position of the furan ring may be a good site for improvement of compound 3 activity by addition of hydrogen acceptor like nitrogen atom in this position. Moreover, binding of compound 3 can be further stabilized in the ATP-binding pocket by the hydrophobic interactions of its nonpolar groups with the side chains of Tyr36, Val39, Ala52, Lys54, Met105, Phe107, Gly109, Gly111, Leu160, Val170 and Thr309.

In vitro cell-based assays

It has been previously shown that TNIK plays an essential role in Wnt-regulated gene expression and its depletion resulted in the reduction of both TCF4/β-catenin-dependent gene transcription and proliferation of the Wnt/β-catenin dependent colon cancer cell lines[2, 4]. To test the impact of

8

compound 3 and 3a on TNIK-mediated TCF4 transcriptional activity, we measured luciferase activity in H1703 cell line stably transfected with lentiviral vector 7TFP, containing a multiple copies of TCF-binding site upstream of luciferase reporter gene[33]. Additionally, as a positive control, we used ICG-001, the well known small-molecule inhibitor of TCF/β-catenin-mediated transcription, which selectively inhibits β-catenin/CBP interaction[34]. As shown in Fig. 6, TCF4-dependent luciferase activity decreased considerably following ICG-001 treatment. This effect was specific to the TCF/β-catenin -driven transcription and the viability of Wnt-inactive H1703 7TFP cells was not affected. Compounds 3 and 3a decreased neither the TCF4/β-catenin-dependent transcription nor cell viability. On the contrary, dovitinib treatment significantly reduced the luciferase activity and we assumed that it was the effect of reduced viability of H1703 cells rather than a result of specific transcription inhibition. Additionally, in order to determine the impact of compounds 3 and 3a on growth of Wnt/β-catenin signaling dependent colon cancer cells, their influence on HCT116 and LoVo cell viability was tested. The constitutive activation of Wnt/β-catenin pathway is triggered by activating mutations in the β-catenin gene (*CTNNB1*) or inactivating mutations of the adenomatous polyposis coli gene (*APC*) in HCT116 and LoVo cells, respectively[35]. As shown in Fig. 6, in contrast to ICG-001, compounds 3 and 3a did not suppress growth of colon cancer cell lines. Similarly to ICG-001, dovitinib significantly reduced the viability of HCT116 and LoVo cells. Likewise in H1703, this effect is not TNIK-specific, but likely results from inhibition of additional kinases. The observed lack of activity of compounds 3 and 3a in cell-based assay might be a result of their poor cell/membrane permeability. Nevertheless, consistent with our data, it has been shown that inhibition of TNIK kinase activity with potent and selective 4-phenyl-2-phenylaminopyridine-based TNIK inhibitors had minimal impact on either TCF4/β-catenin-mediated transcription or Wnt-dependent cell viability[10]. These findings suggested that the kinase activity of TNIK is less essential for Wnt/β-catenin signaling than it was previously indicated. Therefore, further investigation to elucidate the role of kinase activity of TNIK in activation of Wnt/β-catenin signaling is needed.

9

Conclusions

TNIK kinase appeared to be a promising target for cancer treatment due to its essential role in the activation of canonical Wnt/β-catenin pathway, permanently activated in the majority of colorectal cancers[2, 36]. Previous reports indicated that survival and proliferation of colorectal cancer cells were highly dependent on the presence of TNIK kinase[2, 4, 5].

In the present study, we employed ligand-based virtual screening of The Zelinsky Institute database to discover novel TNIK kinase inhibitors. All 296 structurally diverse molecules were chosen from 500 top-scored compounds for *in vitro* testing of TNIK inhibitory activity. Finally, five molecules were identified that efficiently inhibited the TNIK kinase activity with IC_{50} values ranging from 0.85 to 10.3 μM. These compounds represented novel chemotypes, for which TNIK inhibitory activity has not been previously shown. Among them, the most potent compound 3 (5-(2,5-dichlorophenyl)-*N*-[4-(4-methylpiperazin-1-yl)phenyl]furan-2-carboxamide) inhibited kinase activity of TNIK with IC_{50} = 0.85 μM. According to the molecular docking results, compound 3 binds the ATP-binding site of TNIK kinase, where furan-2-carboxamide fragment forms hydrogen bonds with the hinge region. Additional search for molecules structurally related to this hit led us to the identification of compound 3a (5-(3-chloro-2-methylphenyl)-*N*-(4-sulfamoylphenyl)furan-2-carboxamide), a more potent TNIK inhibitor with IC_{50} = 0.258 μM. Moreover, *in vitro* testing of inhibitory activity against a small panel of exemplary kinases revealed that the hit compounds 3 and 3a displayed a noteworthy selectivity. These furan-2-carboxamide derivatives were further used to test the biological effect of TNIK inhibition of Wnt/β-catenin signaling.

In conclusion, virtual screening of a commercially available database allowed for the identification of a novel TNIK inhibitors with furan-2-carboxamide core. They can serve as valuable scaffold for optimization towards potent and selective small molecule TNIK inhibitors not only for therapeutic application but also for revealing biological role of this kinase.

10

Experimental Section

Construction of the data set

Training data set consisted of 30 active, 36 inactive and 1450 putative inactive compounds against TNIK. Active and inactive compounds against TNIK were selected from ChemBlDb [37] and independently diversified using Morgan 1024 bit fingerprint, with maximum Tanimoto similarity 0.58 and 0.31, respectively. Putative inactive compounds were generated using DUD-E methodology on the DUD-E website[38]. 3D conformation for structures was generated with OpenBabel with MMFF94s force field and protonated for pH 7.4[39]. Three active compounds were used as templates during pharmacophore and fingerprint search: doramapimod, dovitinib and sunitinib.

Pharmacophore search

Three programs were used for pharmacophore search. An initial ensemble of active compounds' conformers for those programs was generated with Confab with RMSD cut off 1.0 Å[40]. Align-it version 1.0.3 was used with default settings. SHAFTS version 2011 was used with "volumeMode" set to expensive and rest settings left default. ShaEP version 1.1.1.983 was used with default settings. Four charge models applied in OpenBabel were tested: EEM, Gasteiger-Marsili, QEq and QTPIE.

Fingerprint search

Tanimoto fingerprint similarity was calculated with OpenBabel (with fingerprints: FP2, FP3, FP4 and MACCS), KNIME[41], RDKit[42] (Morgan, RDKit, Avalon, Layered) and CDK[43] (CDK Standard and Extended, EState and PubChem) nodes.

Molecular docking

Molecular docking was carried out using Autodock Vina version 1.1.2[26]. The crystal structure of the kinase domain of human TNIK kinase with 9-hydroxy-4-phenylpyrrolo[3,4-c]carbazole-

11

1.3(2H.6H)-dione (PDB: 2X7F) was used as reference for docking studies. The protein was prepared using PDB2PQR[44]. The grid box size was set to 22x22x22 Å with centre at the native ligand geometric centre.

Library virtual screening

The Zelinsky Institute database (HTS stock) consisting of > 311k compounds was filtered using Open Babel with filter 190<MW<600 and TPSA<200. The 3D conformation for structures was prepared as described for data set and the EEM partial charges model was applied. The database was screened using ShaEP with dovitinib as an active compound. For 500 top-scored compounds, their Murcko scaffolds were extracted using strip-it[45]. Those scaffolds were compared to internal database of 77 known kinase inhibitors cores to exclude compounds with already known scaffolds. Resulting subset was inspected visually and 296 diverse compounds were selected for further activity evaluation. The selected compounds were dissolved in DMSO and stored at -20°C.

In vitro kinase inhibition assay

All kinases were purchased from Carna Biosciences and inhibitory properties of compounds were evaluated with luminescent ADP-Glo™ Kinase Assay from Promega Corporation according to the manufacturer's protocol. Tested compounds were incubated with recombinant kinases in a 25μl reaction mixture containing 30 μM ATP. The exact reactions' conditions are provided in Supplement Table 4. The activity of tested compounds against each kinase was expressed as the percentage of the residual kinase activity for an indicated concentration of inhibitor. IC_{50} values were calculated using GraphPad Prism version 5. Some of the compounds did not fully inhibit kinase activity of TNIK at high micromolar concentrations, and dose-response curve for % of TNIK activity versus log the compound concentration did not result in a full sigmoidal dose-response curve. Therefore, IC_{50} was determined using interpolation of the value of the compound's concentration corresponding to TNIK inhibition that equals 50%. All the assays were replicated twice.

MedChemComm Accepted Manuscript

Cell lines

Colon cancer cell lines HCT116 and LoVo were purchased from ATCC and DSMZ, respectively. Reporter cell line: H1703 7TFP was generated by transducing NSCLC cancer cell line H1703 purchased from ATCC with lentiviral vector 7TFP containing 7xTcf-FFluc (Firefly Luciferase) reporter cassette (Plasmid 24308, Addgene). HCT116 was cultured in McCoy's 5a medium. LoVo and H1703 7TFP were cultured in RPMI 1640 medium. The media were supplemented with 10% fetal bovine serum and the cells were cultured according to the manufacturer's instructions.

Cell viability assay

For viability assays colon cancer cells were seeded in 96-well plates and treated with tested compounds, ICG-001 (Enzo Life Science) or dovitinib (LC Laboratories) in concentration of 10 μM for 72 hours. Cell viability was determined by ATPlite assay (PerkinElmer).

Luciferase activity assay

For luciferase activity assays, H1703 7TFP cells were seeded in 96-well plates and treated with tested compound for 24 hours. Luciferase activity was measured with the Luciferase Assay System (Promega Corporation). 16 hours prior to luciferase assay Wnt/β-catenin signaling pathway was activated by treating cells with 1.5 μM GSK-3 Inhibitor X (Calbiochem).

Disclosure of Potential Conflicts of Interest

Anna Bujak, Paulina Grygielewicz, Marcin Zagozda, Pawel Gunerka, Krzysztof Dubiel are full-time employees of Celon Pharma Inc. Maciej Wieczorek is Chief Executive Officer of Celon Pharma Inc. Karolina Dzwonek, Filip Stefaniak, Daria Zdzalik, Barbara Dymek, Monika Lamparska-Przybysz were full-time employees of Celon Pharma Inc. during experimental phase of the work. The authors disclose no potential conflicts of interest.

Grant Support

Acknowledgments

Keywords

14

References

1. C. A. Fu, M. Shen, B. C. Huang, J. Lasaga, D. G. Payan and Y. Luo, *The Journal of biological chemistry*, 1999, **274**, 30729-30737.

2. T. Mahmoudi, V. S. Li, S. S. Ng, N. Taouatas, R. G. Vries, S. Mohammed, A. J. Heck and H. Clevers, *The EMBO journal*, 2009, **28**, 3329-3340.

3. T. Yamada, M. Shitashige, K. Yokota, M. Sawa and H. Moriyama, *Journal*, 2010.

4. M. Shitashige, R. Satow, T. Jigami, K. Aoki, K. Honda, T. Shibata, M. Ono, S. Hirohashi and T. Yamada, *Cancer research*, 2010, **70**, 5024-5033.

5. J. Gui, B. Yang, J. Wu and X. Zhou, *Human cell*, 2011, **24**, 121-126.

6. C. Schurch, C. Riether, M. S. Matter, A. Tzankov and A. F. Ochsenbein, *The Journal of clinical investigation*, 2012, **122**, 624-638.

7. A. Shkoda, J. A. Town, J. Griese, M. Romio, H. Sarioglu, T. Knofel, F. Giehler and A. Kieser, *PLoS biology*, 2012, **10**, e1001376.

8. D. H. Yu, X. Zhang, H. Wang, L. Zhang, H. Chen, M. Hu, Z. Dong, G. Zhu, Z. Qian, J. Fan, X. Su, Y. Xu, L. Zheng, H. Dong, X. Yin, Q. Ji and J. Ji, *Oncogenesis*, 2014, **2**, e89.

9. J. Kim, S. H. Moon, B. T. Kim, C. H. Chae, J. Y. Lee and S. H. Kim, *PloS one*, 2014, **9**, e110180.

10. K. K. Ho, K. M. Parnell, Y. Yuan, Y. Xu, S. G. Kultgen, S. Hamblin, T. F. Hendrickson, B. Luo, J. M. Foulks, M. V. McCullar and S. B. Kanner, *Bioorganic & medicinal chemistry letters*, 2013, **23**, 569-573.

11. G. Sliwoski, S. Kothiwale, J. Meiler and E. W. Lowe, Jr., *Pharmacological reviews*, 2014, **66**, 334-395.

12. A. S. Reddy, S. P. Pati, P. P. Kumar, H. N. Pradeep and G. N. Sastry, *Current protein & peptide science*, 2007, **8**, 329-351.

13. A. Lavecchia and C. Di Giovanni, *Current medicinal chemistry*, 2013, **20**, 2839-2860.

14. B. C. Duffy, L. Zhu, H. Decornez and D. B. Kitchen, *Bioorganic & medicinal chemistry*, 2012, **20**, 5324-5342.

15. X. H. Ma, F. Zhu, X. Liu, Z. Shi, J. X. Zhang, S. Y. Yang, Y. Q. Wei and Y. Z. Chen, *Current medicinal chemistry*, 2012, **19**, 5562-5571.

16. S. Z. Grinter and X. Zou, *Molecules*, 2014, **19**, 10150-10176.

17. Y. C. Chen, *Trends Pharmacol Sci*, 2015, **36**, 78-95.

18. E. Yuriev and P. A. Ramsland, *J Mol Recognit*, 2013, **26**, 215-239.

19. C. Acharya, A. Coop, J. E. Polli and A. D. Mackerell, Jr., *Current computer-aided drug design*, 2011, **7**, 10-22.

20. P. Ripphausen, B. Nisius and J. Bajorath, *Drug discovery today*, 2011, **16**, 372-376.

21. A. K. Halder, A. Saha and T. Jha, *Current topics in medicinal chemistry*, 2013, **13**, 1098-1126.

22. G. Hu, G. Kuang, W. Xiao, W. Li, G. Liu and Y. Tang, *Journal of chemical information and modeling*, 2012, **52**, 1103-1113.

23. V. Venkatraman, V. I. Perez-Nueno, L. Mavridis and D. W. Ritchie, *Journal of chemical information and modeling*, 2010, **50**, 2079-2093.

24. P. C. Hawkins, G. L. Warren, A. G. Skillman and A. Nicholls, *Journal of computer-aided molecular design*, 2008, **22**, 179-190.

25. J. F. Truchon and C. I. Bayly, *Journal of chemical information and modeling*, 2007, **47**, 488-508.

26. O. Trott and A. J. Olson, *Journal of computational chemistry*, 2010, **31**, 455-461.

27. M. I. Davis, J. P. Hunt, S. Herrgard, P. Ciceri, L. M. Wodicka, G. Pallares, M. Hocker, D. K. Treiber and P. P. Zarrinkar, *Nature biotechnology*, 2011, **29**, 1046-1051.

28. J. Taminau, G. Thijs and H. De Winter, *Journal of molecular graphics & modelling*, 2008, **27**, 161-169.

16

29. X. Liu, H. Jiang and H. Li, *Journal of chemical information and modeling*, 2011, **51**, 2372-2385.

30. M. J. Vainio, J. S. Puranen and M. S. Johnson, *Journal of chemical information and modeling*, 2009, **49**, 492-502.

31. X. Huang, G. W. Shipps, Jr., C. C. Cheng, P. Spacciapoli, X. Zhang, M. A. McCoy, D. F. Wyss, X. Yang, A. Achab, K. Soucy, D. K. Montavon, D. M. Murphy and C. E. Whitehurst, *ACS medicinal chemistry letters*, 2011, **2**, 632-637.

32. F. Andre, T. Bachelot, M. Campone, F. Dalenc, J. M. Perez-Garcia, S. A. Hurvitz, N. Turner, H. Rugo, J. W. Smith, S. Deudon, M. Shi, Y. Zhang, A. Kay, D. G. Porta, A. Yovine and J. Baselga, *Clinical cancer research : an official journal of the American Association for Cancer Research*, 2013, **19**, 3693-3702.

33. M. Mazur, A. Bujak, M. Matloka, S. Janowska, P. Gunerka, L. Bojarski, A. Stanczak, A. Klejman, A. Bednarek, M. Lamparska-Przybysz and M. Wieczorek, *Analytical biochemistry*, 2015, DOI: 10.1016/j.ab.2015.01.016.

34. M. Eguchi, C. Nguyen, S. C. Lee and M. Kahn, *Medicinal chemistry*, 2005, **1**, 467-472.

35. COSMIC: catalogue of somatic mutations in cancer: http://cancer.sanger.ac.uk/cancergenome/projects/cosmic/) (access February 2014).

36. J. Behrens, *Biochemical Society transactions*, 2005, **33**, 672-675.

37. A. Gaulton, L. J. Bellis, A. P. Bento, J. Chambers, M. Davies, A. Hersey, Y. Light, S. McGlinchey, D. Michalovich, B. Al-Lazikani and J. P. Overington, *Nucleic acids research*, 2012, **40**, D1100-1107.

38. M. M. Mysinger, M. Carchia, J. J. Irwin and B. K. Shoichet, *Journal of medicinal chemistry*, 2012, **55**, 6582-6594.

39. N. M. O'Boyle, M. Banck, C. A. James, C. Morley, T. Vandermeersch and G. R. Hutchison, *Journal of cheminformatics*, 2011, **3**, 33.
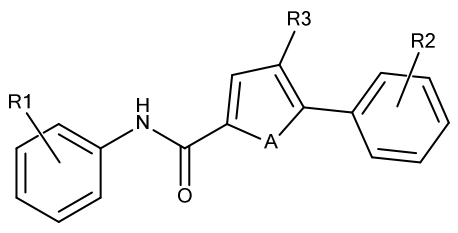
17

40. N. M. O'Boyle, T. Vandermeersch, C. J. Flynn, A. R. Maguire and G. R. Hutchison, *Journal of cheminformatics*, 2011, **3**, 8.

41. C. N. Berthold M. R., DIll F., Gabriel R. T., Kotter T., Meinl T., Ohl P., Sieb C., Thiel K., Wiswedel B., in *Data Analysis, Machine Learning and Applications*, 2008, DOI: 10.1007/978-3-540-78246-9_38, ch. 319-326.

42. RDKit: Open-source cheminformatics: http://www.rdkit.org (access February 2014).

43. C. Steinbeck, Y. Han, S. Kuhn, O. Horlacher, E. Luttmann and E. Willighagen, *Journal of chemical information and computer sciences*, 2003, **43**, 493-500.

44. T. J. Dolinsky, J. E. Nielsen, J. A. McCammon and N. A. Baker, *Nucleic acids research*, 2004, **32**, W665-667.

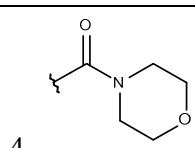45. Strip-it by Silicos-it http://silicos-it.com/software/strip-it/1.0.2/strip-it.html) (access February 2014).
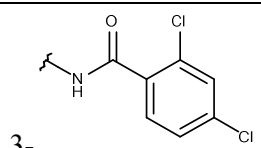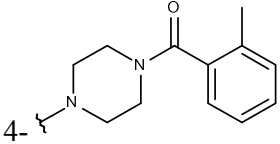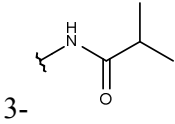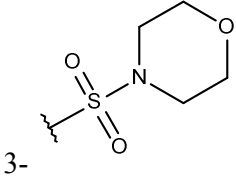
18
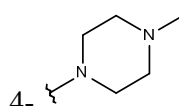
Tables

Table 1. TNIK inhibitory activities of newly discovered inhibitors. The corresponding structures are shown in Fig. 3.

compound	MW	%inh@10μM	IC$_{50}$ [μM]	PEI
1	297.06	70±6.2	3.57	2.37
2	343.14	79±4.5	10.31	2.30
3	429.10	94±10.6	0.85	2.19
4	322.17	63±3.7	2.74	1.95
5	373.08	72±2.1	3.51	1.92
6	277.11	43±7.7	ND	1.57
7	279.10	40±14.6	ND	1.44
8	280.12	39±4.4	ND	1.39
9	329.13	45±11	ND	1.37
10	327.16	42±1	ND	1.27
11	377.17	46±7.6	ND	1.23
12	281.14	32±0.3	ND	1.15

PEI: Potency Efficiency Index; PEI=TNIK inhibition at 10 μM (as fraction 0-1)/molecular weight (kDa)

MedChemComm Accepted Manuscript

19

Table 2. The structural analogs of the compound 3 and their TNIK inhibitory activities.

Compound	R1	R2	R3	A	MW	%inh@10μM	IC$_{50}$ [μM]	PEI
3	4-	2,5-di-Cl	H	O	429.10	93.9	0.85	2.19
3a	4-(NH$_2$SO$_2$-)	2-Me,3-Cl	H	O	390.04	76.4	0.26	1.96
3b	4-(MeNHSO$_2$-)	H	Me	S	386.08	72.8	ND	1.89
3c	2-(NH$_2$C(O)-)	H	Me	S	336.09	61.7	ND	1.84
3d	4-	H	Me	S	406.14	60.4	ND	1.49
3e	4-(AcNH-)	3,4-di-Cl	H	O	388.04	23.1	ND	0.60
3f	2-Cl	4-Cl	H	O	331.02	18.7	ND	0.56
3g	3-Cl,2-(N-morpholine)	2-Me,4-NO$_2$	H	O	441.11	22.3	ND	0.51
3h	3-Cl,4-(N-piperidine)	4-F	H	O	398.12	19.9	ND	0.50
3i	3-	3-NO$_2$	H	O	495.04	16.8	ND	0.34

20

3j	4-	4-Cl	H	O	499.17	12.9		ND	0.26
3k	3,5-di-Cl	4-NO$_2$	H	O	376.00	8.9		ND	0.24
3l	2-Me,4-NO2	2,3-di-Cl	H	O	390.02	4.9		ND	0.13
3m	3-	4-Cl	H	O	382.11	4.1		ND	0.11
3n	3-	H	Me	S	442.10	-4.9		ND	-0.11

PEI: Potency Efficiency Index; PEI=TNIK inhibition at 10μM (as fraction 0-1)/molecular weight

(kDa)

21

Table 3. The selectivity profiles of the compounds 3 and 3a. Percent (%) of inhibition was determined in the presence of 30 μM ATP and 10 μM compound 3 or 3a using *in vitro* kinase inhibition assay. The reactions' conditions are listedin the Supplementary Table S4. Values represent the means ± SD of two 2 independent experiments.

Kinase	% of inhibition	
	Compound 3	Compound 3a
ALK	17.4 ± 5.8	18.4 ± 14.2
AURA	19.5 ± 1.4	17.4 ± 4.3
BTK	4.3 ± 7.2	-2.3 ± 11.3
EGFR	9.3 ± 3.5	51.7 ± 2.0
FGFR1	21.6 ± 5.9	5.2 ± 9.1
FGFR2	54.8 ± 11.9	32.4 ± 7.8
FLT3	93.8 ± 3.0	27.0 ± 0.4
GSK3	20.7 ± 14.6	17.3 ± 4.2
IGF-1R	3.4 ± 4.0	7.7 ± 6.1
JAK2	3.5 ± 7.9	23.7 ± 8.3
KDR	64.9 ± 6.7	0.1 ± 14.0
PDGFRβ	75.7 ± 6.8	13.8 ± 11.9
PI3Kα	11.7 ± 8.9	-25.9 ± 6.6
PIM1	46.9 ± 10.5	24.0 ± 5.1
SYK	34.9 ± 2.4	15.3 ± 13.5

22

Figure legends

Figure 1. Performance of screening with methods used on testing dataset. For ligand based methods (2D and 3D) the values obtained for the best template (dovitinib) are shown.
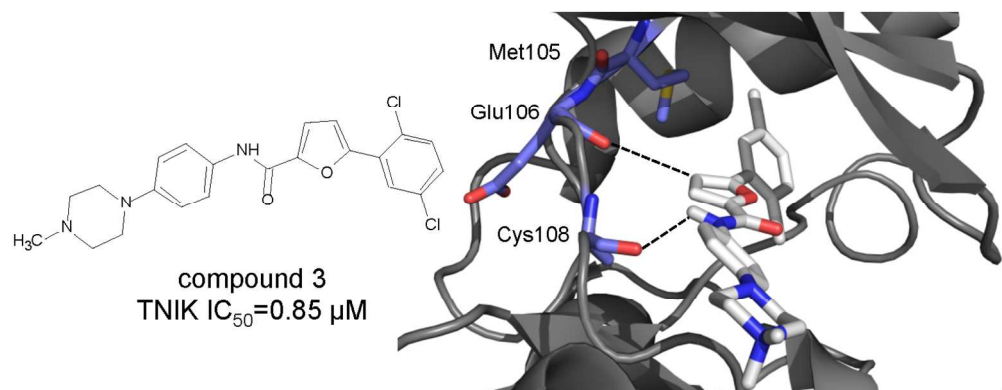
Figure 2. Kinase inhibitors used as templates in the ligand-based methods benchmark. The dissociation constant (K_d) values for TNIK kinase are shown.

Figure 3. Structures of newly discovered TNIK inhibitors. The corresponding data are summarized in Table 1.

Figure 4. The inhibitory activity of dovitinib (A), compound 3 (B) and compound 3a (C) against TNIK kinase. Activities of dovitinib and compound 3 were tested in the presence of increasing ATP concentration. The corresponding IC_{50} values are shown in brackets. The compound 3a was tested in the presence of 30 μM ATP.

Figure 5. Predicted binding mode of compound 3 within ATP-binding site of TNIK obtained by molecular docking. TNIK is shown in gray cartoon representation (PDB ID 2X7F). Residues Glu106 and Cys108, providing the most important hydrogen bonds with the compound, and gatekeeper residue Met105 in the hinge region are shown as a stick model, colored by element type (C in slate, O in red, and N in blue). Hydrogen bonds between ligand and enzyme are displayed as the dotted lines. Compound 3 is shown as a stick model, colored by element type (C in white, O in red, and N in blue, Cl in green).

Figure 6. The impact of dovitinib, ICG-001, compounds 3 and 3a on TCF4/β-catenin-dependent transcription (A) and viability of Wnt-activated colorectal cancer cells (B). A. Luciferase activity and cell viability were measured following 24-hour incubation of H1703 7TFP reporter cell line with studied compounds at final 10 μM concentration. Wnt/β-catenin signaling was activated by GSK-3β inhibition prior to addition of tested compounds treatment. Values represent the means ± SD of two independent experiments. B. Cell viability was assayed by ATPlite assay following 72-hours incubation with studied compounds at 10 μM concentration. Values represent the means ± SD of two 2 independent experiments.

23

compound 3
TNIK IC$_{50}$=0.85 μM

129x50mm (300 x 300 DPI)